ELSEVIER

Journal of Alloys and Compounds 434–435 (2007) 614–617

Journal of ALLOYS AND COMPOUNDS

www.elsevier.com/locate/jallcom

Magnetic properties and structure of Fe–Pt–M–B (M = Zr, Nb and Ti) alloys produced by quenching technique

Akihiro Makino [a,b,*], Teruo Bitoh [a], Akihisa Inoue [b], Yoshihiko Hirotu [c]

[a] *Department of Machine Intelligence and Systems Science, Faculty Systems Science and Technology, Akita Prefectural University, 84-4 Ebinokuchi, Tuchiya, Yurihonjo 015-0055, Japan*

[b] *Advanced Research Center of Metallic Glasses, Institute for Materials Research, Tohoku University, 2-1-1 Katahira, Aoba-ku, Sendai 980-8577, Japan*

[c] *The Institute of Scientific and Industrial Research, Osaka University, 8-1 Mihogaoka, Ibaraki 567-0047, Japan*

Available online 19 December 2006

Abstract

The $L1_0$–FePt nanocrystalline phase is directly formed by the rapid quenching of the $(Fe_{0.55}Pt_{0.45})$–M–B (M = Zr, Nb and Ti) alloy melt. The as-quenched alloys exhibit coercivity higher than 200 kA/m. The direct formation of $L1_0$–FePt takes place at the compositional range where the equilibrium disordered fcc phase disappears by decreasing of melting temperature into the $L1_0$–FePt phase stable region with simultaneous addition of the M elements and B, presumably because of the strong interaction of Pt–M pairs.

Keywords: Permanent magnets; Liquid quenching; Nanostructures; Magnetic measurements; Calorimetry

1. Introduction

The ordered $L1_0$–FePt alloy has long been anticipated as materials for permanent magnets because of large magnetic anisotropy ($K_u = 7 \times 10^6$ J/m^3 [1]) and good corrosion resistance. However, near equiatomic FePt cast alloys do not exhibit high magnetic hardness because of their coarsening structure [2]. On the other hand, the structure of the as-made FePt thin films produced by vapor-quenching technique is generally disordered fcc with low coercivity (H_c). Heating a substrate during deposition and/or post-annealing is necessary to obtain the $L1_0$ phase with high H_c [3–7]. However, high-temperature annealing should cause grain growth, which results in a low H_c.

Recently, it was found that the melt-spun Fe-rich $(Fe_{0.75}Pt_{0.25})$–B alloys with 20 at.% B or more have a single amorphous structure or a mixed structure of amorphous and nanoscale fcc-FePt. A nanocomposite structure consisting of $L1_0$–FePt, fcc-Fe and Fe_2B was obtained after annealing [8,9]. The present paper considers the effect of simultaneous addition of transition metals (M = Zr, Nb and Ti) and B to near-equiatomic FePt alloys on melting (T_m) and order–disorder transformation (T_{tr}) temperatures. These transition elements have larger atomic radii [10] than Fe and Pt and exhibit large negative mixing enthalpy between Pt [11], as shown in Table 1. The formation of the $L1_0$–FePt phase and the magnetic hardness of the melt-spun alloys are also described.

2. Experimental procedure

Alloy ingots, which are termed as the Cu mold cast alloys in this paper, were prepared by arc melting in an Ar atmosphere. A single-roller melt-spinning method in an Ar atmosphere was used to produce rapidly solidified alloys. The structure of the samples was examined by powder X-ray diffractometry (XRD) and transmission electron microscopy (TEM). Magnetic properties were measured using either a vibrating sample magnetometer (VSM) with a maximum field (H_m) of 1 MA/m or a superconducting quantum interference device (SQUID) magnetometer with an H_m value of 4 MA/m. Thermal properties were examined by a differential scanning calorimeter (DSC) with a heating rate of 0.17 K/s.

3. Results and discussion

3.1. $(Fe_{0.55}Pt_{0.45})$–Zr–B alloys

First, the effect of the simultaneous addition of Zr and B to the $Fe_{55}Pt_{45}$ alloy, which is the center of the region where the

* Corresponding author at: Department of Machine Intelligence and Systems Science, Faculty Systems Science and Technology, Akita Prefectural University, 84-4 Ebinokuchi, Tuchiya, Yurihonjo 015-0055, Japan. Tel.: +81 184 27 2161; fax: +81 184 27 2161.

E-mail address: akihiro_makino@akita-pu.ac.jp (A. Makino).

0925-8388/$ – see front matter © 2006 Elsevier B.V. All rights reserved.
doi:10.1016/j.jallcom.2006.08.092

Table 1
Mixing enthalpy [11] and Goldschmidt atomic radius [12] of the constitute elements

	Mixing enthalpy, ΔH_{mix} (kJ/mol)			Atomic radii, r (nm)
	Fe	Pt	B	
Fe	–	–	–	0.126
Pt	−13	–	–	0.138
B	−11	−13	–	0.097
Ti	−17	−74	−43	0.147
Zr	−25	−100	−56	0.160
Nb	−16	−67	−39	0.147

$L1_0$–FePt phase is formed [12], was investigated. Fig. 1 shows the compositional dependence of H_c and the structure for the melt-spun $(Fe_{0.55}Pt_{0.45})$–Zr–B alloys in an as-quenched state. The mixed structure of disordered fcc and ordered $L1_0$–FePt phases is formed in the compositional range 2–8 at.% Zr and 15–24 at.% B. The structure composed of the $L1_0$–FePt phase with a minor segment of the fcc phase (approximately 30 vol.% [13]) is formed in the compositional range 2–5 at.% Zr and 17–20 at.% B where the H_c higher than 200 kA/m is obtained. TEM observation reveals that the structure of melt-spun $(Fe_{0.55}Pt_{0.45})_{78}Zr_4B_{18}$ alloy, which exhibits the highest H_c of 649 kA/m among the $(Fe_{0.55}Pt_{0.45})$–Zr–B alloys, is mainly composed of $L1_0$–FePt grains with sizes of approximately 80 nm [14,15], smaller than the critical single domain size (≈340 nm) [16]. The coercivity of the $(Fe_{0.55}Pt_{0.45})_{78}Zr_4B_{18}$ alloy is much higher than that of the annealed bulk $Fe_{61.5}Pt_{38.5}$ [2] and melt-spun $(Fe_{0.65}Pt_{0.35})_{83}B_{17}$ [17] alloys previously reported. On the other hand, most of the Cu mold cast alloys are mainly composed of compound phases and do not exhibit high H_c; the maximum H_c was obtained for the binary $Fe_{55}Pt_{45}$ with a single $L1_0$–FePt structure [14,15].

With increase in B content, T_m of the $(Fe_{0.55}Pt_{0.45})$–Zr–B alloys drastically decreases; the lowest T_m is 1360 K for $(Fe_{0.55}Pt_{0.45})_{78}Zr_4B_{18}$. This T_m is as much as 473 K lower than the 1833 K of $Fe_{55}Pt_{45}$ [12], and is also lower than T_{tr} at 1548 K for the binary alloy [12]. As already reported [15], in the compositional range indicated by gray color in Fig. 1, order–disorder transformation is not observed in the DSC curve, i.e., the melt-spun $L1_0$–FePt phase is stable up to T_m. This compositional range is found to be almost in agreement with that in which T_m is lower than approximately 1400 K [15]. Judging from T_m–T_{tr} (=289 K) for $(Fe_{0.55}Pt_{0.45})_{78}B_{22}$, T_{tr} is also largely decreased by the addition of approximately 20 at.% B. However, the decrease in T_{tr} is suppressed by the simultaneous addition of 2–6 at.% Zr.

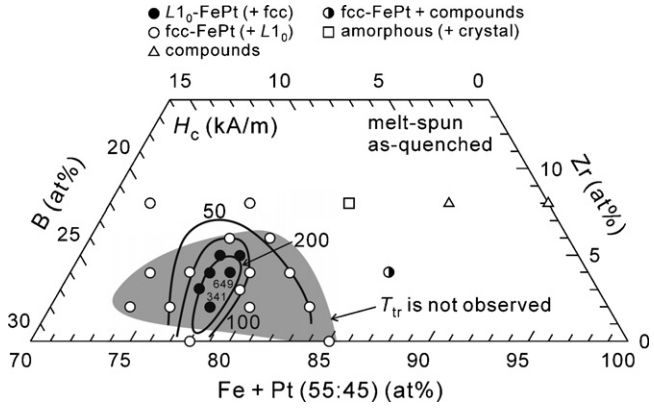

Fig. 1. Compositional dependence of H_c and structure of melt-spun $(Fe_{0.55}Pt_{0.45})$–Zr–B alloys in an as-quenched state.

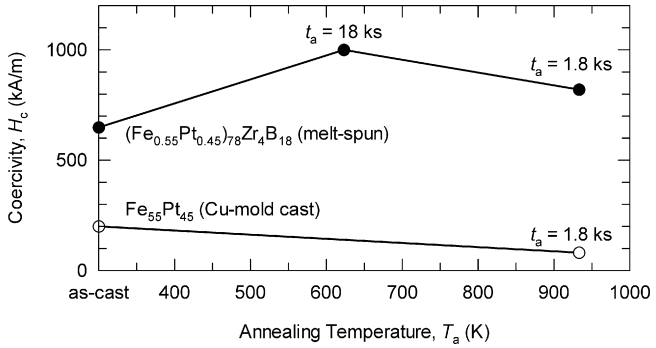

Fig. 2. Annealing temperature dependence of coercivity of melt-spun $(Fe_{0.55}Pt_{0.45})_{78}Zr_4B_{18}$ and Cu mold cast $Fe_{55}Pt_{45}$ alloys. t_a denotes the annealing time.

Fig. 2 shows the annealing temperature dependence of H_c for binary $Fe_{55}Pt_{45}$ and the melt-spun $(Fe_{0.55}Pt_{0.45})_{78}Zr_4B_{18}$ alloys. H_c of the melt-spun alloy increases and reaches to 1000 kA/m after annealing at 623 K for 18 ks, while that of the Cu mold cast alloy considerably decreases by annealing. This result indicates that the $L1_0$–FePt structure directly formed by the melt spinning should not substantially change with annealing; the XRD profile of the annealed (at 923 K for 1.8 ks) alloy is almost the same as that of the as-quenched alloy. Therefore, melt-spun $L1_0$–FePt structure has a higher thermal stability than that of Cu mold cast $Fe_{55}Pt_{45}$ alloy despite the melt-spun $L1_0$–FePt being metastable.

3.2. $(Fe_{0.55}Pt_{0.45})$–Nb–B alloys

Fig. 3 shows the compositional dependence of H_c and the structure for the melt-spun $(Fe_{0.55}Pt_{0.45})$–Nb–B alloys in as-quenched state. T_m and T_{tr} could not be measured in the upper region of the broken line because they are too high. The as-quenched structure is mainly composed of the $L1_0$–FePt phase. It should be noted that the $L1_0$–FePt formation region of the $(Fe_{0.55}Pt_{0.45})$–Nb–B alloys is considerably larger than that of the $(Fe_{0.55}Pt_{0.45})$–Zr–B alloys; i.e., 2–8 at.% Nb and 15–24 at.%

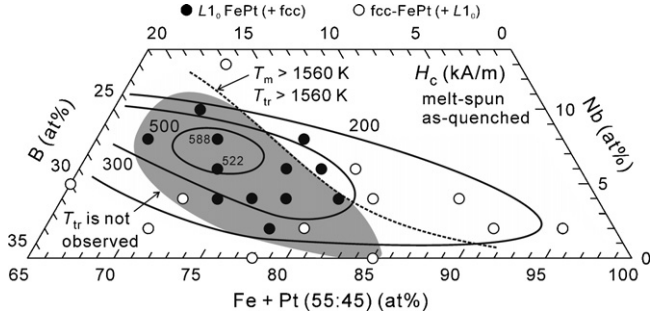

Fig. 3. Compositional dependence of H_c and structure of melt-spun $(Fe_{0.55}Pt_{0.45})$–Nb–B alloys in an as-quenched state.

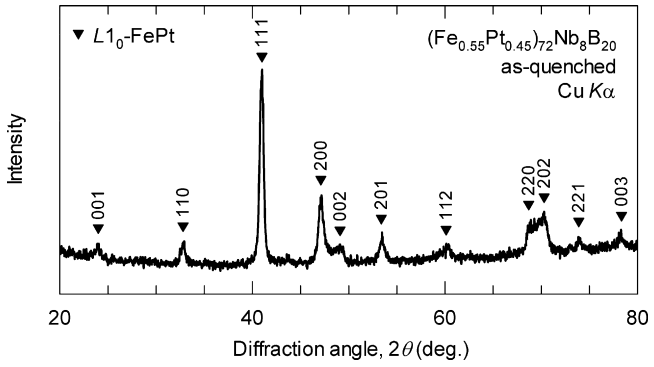

Fig. 4. XRD profile of melt-spun $(Fe_{0.55}Pt_{0.45})_{72}Nb_8B_{20}$ alloy in an as-quenched state.

B, where H_c higher than 300 kA/m is obtained. Figs. 4 and 5 show the XRD profile and the TEM image of the as-quenched $(Fe_{0.55}Pt_{0.45})_{72}Nb_8B_{20}$, respectively. The TEM image reveals that grain size of $L1_0$–FePt is approximately 100 nm. Selected area electron diffraction pattern consists of the distinct diffraction rings of $L1_0$–FePt and the weak rings of the fcc phase, whereas, only diffraction lines from $L1_0$–FePt are observed in the XRD profile. These results indicate that the volume fraction of the fcc phase is much smaller than that of the $(Fe_{0.55}Pt_{0.45})$–Zr–B alloys. Fig. 6 shows DSC curves of the $(Fe_{0.55}Pt_{0.45})_{65}Nb_4B_{31}$ and $(Fe_{0.55}Pt_{0.45})_{65}Nb_6B_{21}$ alloys. The former alloy has as-quenched structure composed of the fcc phase and displays the order–disorder transformation before melting. On the other hand, the order–disorder transformation was not observed for the latter alloy, and the $L1_0$–FePt nanocrystalline structure was directly formed by melt spinning. These results are similar to that of the $(Fe_{0.55}Pt_{0.45})$–Zr–B alloys.

3.3. $(Fe_{0.55}Pt_{0.45})$–Ti–B alloys

Fig. 7 shows the compositional dependence of H_c and the structure for the melt-spun $(Fe_{0.55}Pt_{0.45})$–Ti–B alloys in as-quenched state. Fig. 8 shows the XRD profile of as-quenched $(Fe_{0.55}Pt_{0.45})_{83}Ti_2B_{15}$. The structure is mainly composed of $L1_0$–FePt phase with grain size of approximately 100 nm and

Fig. 5. TEM image and selected area electron diffraction pattern of melt-spun $(Fe_{0.55}Pt_{0.45})_{72}Nb_8B_{20}$ alloy in an as-quenched state.

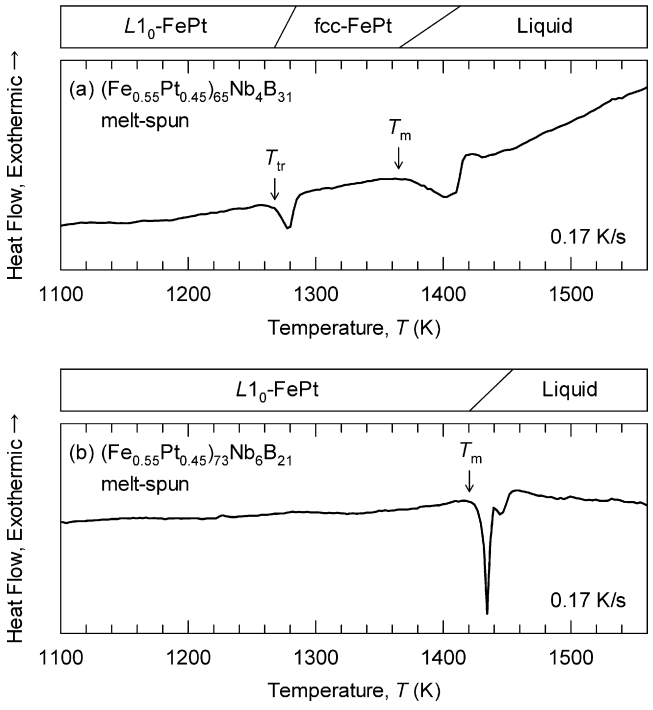

Fig. 6. DSC curves of melt-spun: (a) $(Fe_{0.55}Pt_{0.45})_{65}Nb_4B_{31}$ and (b) $(Fe_{0.55}Pt_{0.45})_{65}Nb_6B_{21}$ alloys.

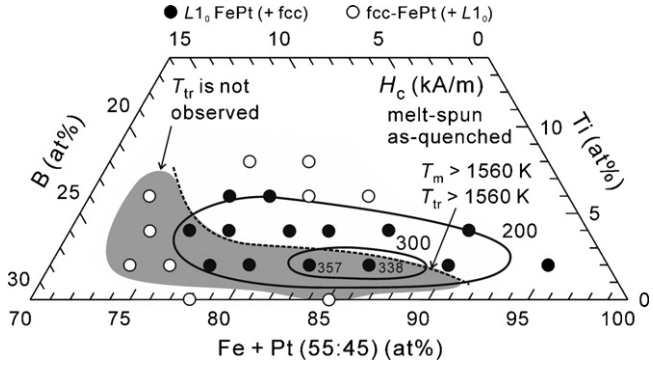

Fig. 7. Compositional dependence of H_c and structure of melt-spun $(Fe_{0.55}Pt_{0.45})$–Nb–B alloys in an as-quenched state.

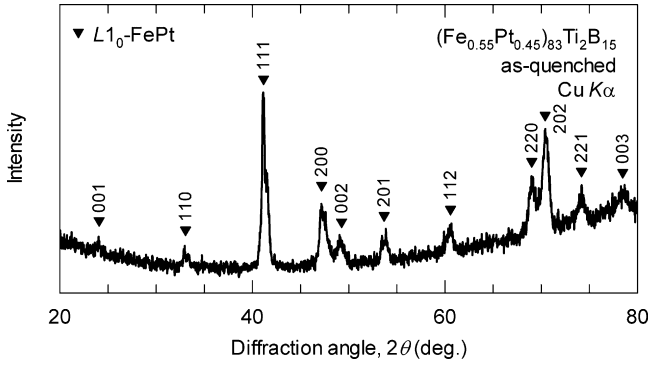

Fig. 8. XRD profile of melt-spun $(Fe_{0.55}Pt_{0.45})_{83}Ti_2B_{15}$ alloy in an as-quenched state.

H_c higher than 200 kA/m is obtained in the wide compositional range of 2–6 at.% Ti and 3–20 at.% B. It should be noted that the $L1_0$–FePt formation range is located in the FePt-rich composition as compared with that of the $(Fe_{0.55}Pt_{0.45})$–(Zr or Nb)–B alloys.

4. Conclusion

The simultaneous addition of the M elements and B to near equiatomic FePt alloys strongly decreases T_m. The T_{tr} is also strongly decreased by the addition of B, however, the decrease in T_{tr} is suppressed by the simultaneous addition of the M elements. Direct formation of $L1_0$ by rapid quenching takes place at the compositional range where the fcc region, which at equilibrium exists between liquid and the $L1_0$–FePt phase region at near equiatomic composition in Fe–Pt system, disappears by the decrease of T_m by simultaneous addition of the M elements and B, presumably because of the strong interaction of Pt–M pairs. These results suggest that rapidly quenching the melt is useful to realize good hard magnetic properties through grain size refinement in near equiatomic FePt alloys.

References

[1] O.A. Ivanov, L.V. Solina, V.A. Demshina, L.M. Magat, Phys. Met. Metallogr. 35 (1973) 81–85.
[2] K. Watanabe, H. Masumoto, Trans. Jpn. Inst. Met. 20 (1983) 627–632.
[3] T. Shima, T. Moriguchi, S. Mitani, K. Takanashi, Appl. Phys. Lett. 80 (2002) 288–290.
[4] K. Sato, M. Fujiyoshi, M. Ishimaru, Y. Hirotu, Scripta Mater. 48 (2003) 921–927.
[5] C.P. Luo, D.J. Sellmyer, IEEE Trans. Magn. 31 (1995) 2764–2766.
[6] Y. Endo, N. Kikuchi, O. Kitakami, Y. Shimada, J. Appl. Phys. 89 (2001) 7065–7067.
[7] H. Yamaguchi, O. Kitakami, S. Okamoto, Y. Shimada, K. Oikawa, K. Fukamichi, Appl. Phys. Lett. 79 (2001) 2001–2003.
[8] W. Zhang, D.V. Louzguine, A. Inoue, Appl. Phys. Lett. 85 (2004) 4998–5000.
[9] A. Inoue, W. Zhang, T. Tsurui, D.V. Louzguine, Mater. Trans. 46 (2005) 891–894.
[10] C.J. Smithells, E.A. Brandes, G.B. Brook, Smithells Metals Reference Book, 7th ed., Butterworth-Heinemann, Boston, 1992.
[11] F.R. de Boer, R. Boom, W.C.M. Mattens, A.R. Miedema, A.K. Niessen, Cohesion in Metals, North-Holland, Amsterdam, 1988.
[12] T.B. Massalski, H. Okamoto, Binary Alloy Phase Diagrams, 2nd ed., ASM, Materials Park, 1990.
[13] T. Bitoh, A. Makino, J. Appl. Phys. 97 (2005) 10H307.
[14] A. Makino, T. Bitoh, J. Appl. Phys. 95 (2004) 7498–7500.
[15] A. Makino, T. Bitoh, A. Inoue, Mater. Trans. 45 (2004) 2909–2915.
[16] T. Klemmer, D. Hoydick, H. Okumura, B. Zhang, W.A. Soffa, Sci. Metall. Mater. 33 (1995) 1793–1805.
[17] K. Inomata, T. Sawa, S. Hashimoto, J. Appl. Phys. 64 (1988) 2537–2540.